Journal of Structural Geology, Vol. 12, No. 4, pp. 471 to 481, 1990
Printed in Great Britain

0191-8141/90 $03.00+0.00

Curved slickenfibers: a new brittle shear sense indicator with application to a sheared serpentinite

ROBERT J. TWISS and MICHAEL J. GEFELL*

Geology Department, University of California at Davis, Davis, CA 95616, U.S.A.

(*Received* 3 *July* 1989; *accepted in revised form* 3 *December* 1989)

Abstract—Brittle fault zones are commonly characterized by penetrative fracturing of the rock to form an aggregate of blocks, so that the rock becomes, in essence, like a granular material composed of rigid 'grains'. The surfaces of the blocks, or 'grains', have a wide distribution of orientations, and shearing of the blocks past one another on these planes accommodates the large-scale motion, i.e. the macromotion, in the fault zone. During a macromotion that is a non-coaxial deformation, the rigid blocks and their surfaces may undergo a progressive rigid rotation that is distinct from the macromotion and is described by the microspin. If a macroscopic non-coaxial deformation has monoclinic symmetry, this symmetry should be reflected in the sense of rigid rotation of the blocks and their surfaces.

On the surfaces of the blocks, which are local shear planes, the history of displacement may be recorded by mineral fibers that grow progessively with displacement. Because of the rigid rotation of the local shear planes, slickenfiber lineations commonly are curved. The sense of curvature from the youngest to the oldest part of the fiber, looking down the normal to the local shear plane, is different for those planes whose normals are on opposite sides of the unique monoclinic symmetry plane for the macroscopic shearing. The intersection of the symmetry plane with the plane of the fault zone defines the macroscopic slip direction, and the sense of rigid rotation of the local shear planes determined from the lineations defines the shear sense.

Application of this technique to the disrupted and sheared margins of the Feather River Peridotite in the northern Sierra Nevada of California indicates that late deformation involved dextral-normal oblique slip along the Melones fault zone.

INTRODUCTION

IN RECENT years, the development of techniques for using microstructures to infer the shear sense in major ductile shear zones (e.g. Berthé *et al.* 1979, Platt & Vissers 1980, Simpson & Schmid 1983, Lister & Snoke 1984, Passchier & Simpson 1986) has enabled the interpretation of tectonic displacements that previously were obscure or unknown. The shear sense on brittle faults can also be deduced from the characteristics of fractures and microfractures associated with the fault (Hancock 1985, Petit 1987). In this paper, we present a new method that lends itself to simple field application, by which the macroscopic shear sense can be deduced for a brittle fault zone containing curved slickenfiber lineations on multiple local shear surfaces.

Large-scale fault zones commonly are penetratively fractured into an aggregate of blocks whose surfaces have a wide distribution of orientations. The rock is essentially a macro-granular material in which the large-scale simple shear in the fault zone, referred to as the macromotion, is accommodated by the sliding of the blocks past one another on their surfaces. The surfaces of the blocks thereby become local shear planes. Marshak *et al.* (1982) refer to this type of deformation as "mesoscopic cataclasis", and it has been recognized in numerous instances (see references in Marshak *et al.* 1982). We assume that the blocks, and therefore the local shear planes that make up their surfaces, also undergo a progressive rigid rotation during the deformation. The rigid rotation rate of the blocks, which we call the microspin, is distinct from the macromotion but reflects the macroscopic sense of shear.

We postulate that the curved slickenfibers result from the growth of fibers during macroscopic faulting and the associated local rigid rotation of the blocks and their surfaces. The sense of curvature of slickenfibers (clockwise or counterclockwise) about the pole to the local shear plane in which they lie, depends on the orientation of the local shear plane pole relative to the microspin axis. The orientation of the microspin axis in turn reflects the monoclinic symmetry of the macroscopic shearing in the fault zone. Thus we can use the curvature sense of the slickenfibers on surfaces of many different orientations to constrain the geometry of the macroscopic deformation.

Our model is summarized in Fig. 1, where for simplicity we show a single rigid octahedral block whose faces are the local shear planes. For convenience of illustration, we show the block with its surfaces arranged symmetrically with respect to the symmetry plane for the macroscopic simple shear and with respect to the normal to the macroscopic fault plane. The history of the displacement directions of material across the faces of the block is indicated by the curved arrows and is recorded by slickenlines that may develop on the faces. The directions become younger towards the arrowhead. When viewed *looking down on the local shear plane*, the sense of slickenline curvature indicated by these arrows is different for shear plane poles that lie on opposite sides of the symmetry plane for the macroscopic simple

*Present address: Blasland, Bouck, and Lee, Inc., Engineers and Geoscientists, 6723 Towpath Road, Box 66, Syracuse, NY 13214, U.S.A.

shear (cf. arrows on planes that are inclined to the left of the symmetry plane with those on planes that are inclined to the right in Fig. 1, remembering to determine curvature sense looking down on the plane).

Thus we can use measurements of the sense of slickenline curvature on local shear planes of widely distributed orientations to deduce the orientation of the symmetry plane for the macroscopic shear in brittle fault zones. Because the intersection of the symmetry plane with the plane of faulting defines the slip direction (Fig. 1), and the sense of curvature of the slickenlines defines the sense of shear (Fig. 1), we can infer both the direction and sense of shear in the fault zone. The technique is comparable to Hansen's (1971) method for deducing slip direction and shear sense from the asymmetry of minor folds in ductile shear zones.

Sheared serpentinites commonly are penetratively fractured into distinct blocks whose sheared surfaces are covered by mineral fiber lineations (slickenfibers) of widely varying orientation. The margins of the Feather River Peridotite in the northern Sierra Nevada of California provide one example, and we illustrate this technique by applying it to the interpretation of late motion along the faults bounding the peridotite body (Gefell 1989, Gefell *et al.* 1989).

This analysis is applied in particular to slickensides containing slickenfibers, for we are most confident of the interpretation of their origin (Durney & Ramsay 1973, Ramsay 1980, Ramsay & Huber 1983). In principle, however, the same technique should be applicable to any set of slickenlines that lengthen progressively during a finite deformation. Some slickenlines, such as ridge-and-groove lineations (Means 1987), may not meet this criterion, and slickenlines generated during a relatively instantaneous (seismic) slip event also may not.

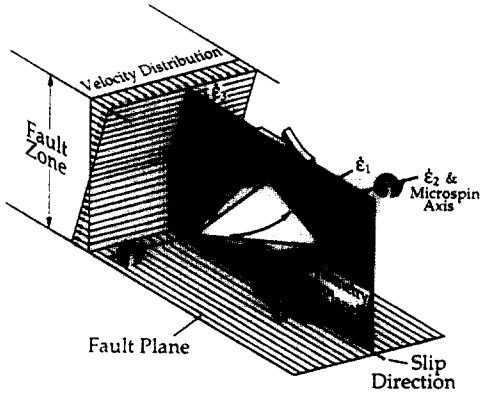

Fig. 1. Geometry of simple shear, microspin and curved slickenlines in a fault zone. The velocity distribution indicates macroscopic progressive simple shear parallel to the fault zone. Slip direction is parallel to the intersection line of the symmetry plane for macroscopic motion with the fault zone orientation. A rigid octahedral block rotates progressively during deformation about the axis of microspin normal to the symmetry plane. For convenience of illustration, surfaces of the block are symmetrically disposed with respect to the symmetry plane, and the block is shown at the instant when its planes are symmetrically arranged about the normal to the fault zone. Curved arrows on the surfaces suggest expected pattern of shear directions of material across them resulting from the history of microspin. Arrows are drawn from oldest to youngest directions of shear, and reflect the curvature of slickenlines that would form. Only one plane of symmetry exists for the slickenline pattern. Principal axes of instantaneous strain rate $\dot{\varepsilon}_1$ and $\dot{\varepsilon}_3$ are parallel to the symmetry plane, and $\dot{\varepsilon}_2$ is normal to it. The axis of microspin is parallel to $\dot{\varepsilon}_2$.

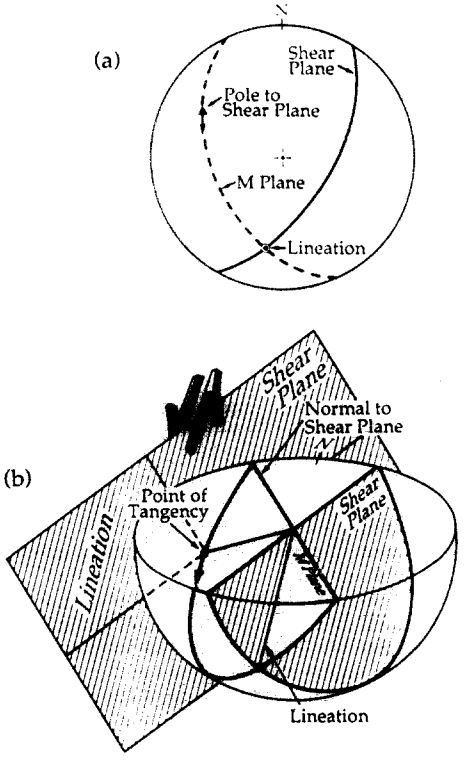

Fig. 2. Construction and interpretation of a tangent-lineation diagram. Plotting slickenline data on a spherical projection requires combining lineation orientation with attitude of plane in which lineation lies. (a) Pole to shear plane is plotted, and a line is constructed through the pole tangent to the great circle (M plane) containing pole and lineation orientation in the shear plane. Directional information associated with the lineation, if available, is indicated by arrowhead, which points in direction of relative motion of footwall block. Note that both equal-angle and equal-area projections distort true trend of lineation. There would be no distortion on an orthographic projection. (b) A three-dimensional interpretation of the tangent-lineation diagram. Pole to shear plane is point at which shear plane would be tangent to the outside of plotting hemisphere. Arrow thus can be interpreted as lineation orientation lying in tangent shear plane, and it points in the direction in which material outside plotting hemisphere moves past hemisphere on tangent shear plane.

Complete information about the orientation of slickenlines requires both the orientation of the shear plane and the orientation of the lineation. These data are conveniently combined in an uncluttered and easily interpreted stereonet diagram that we refer to in a general sense as a 'tangent-lineation diagram' (Fig. 2). These diagrams are constructed by plotting the pole to each local shear plane, and constructing a line through the pole tangent to the great circle (the M plane) that connects the pole to the orientation of the lineation in the shear plane (Fig. 2a) (this technique is attributed to Hoeppener 1955, in Goldstein & Marshak 1988). If directional information is available for the lineation, we plot an arrowhead on the line through the pole so that it indicates the direction of motion of the *footwall* relative to the hanging wall of the shear plane (Fig. 2).

We can interpret a tangent-lineation diagram easily by viewing the shear plane pole as the point where the shear plane is *tangent* to the *outside* of the plotting hemisphere (Fig. 2b). The line or arrow representing the lineation

then lies in the tangent plane and is parallel to the actual orientation of the lineation on that plane. For slickenlines, the pattern of arrows for multiple shear plane orientations (cf. Fig. 4) indicates the directions of motion of material past the lower plotting hemisphere on shear planes tangent to the hemisphere.

Our arrow convention is the opposite of that used by other authors (e.g. Goldstein & Marshak 1988), because the intuitive understanding of the resulting diagram seems easier. We visualize the plotting hemisphere as a stable body imbedded in the deforming medium. The arrows then indicate the direction of motion of the medium past the hemisphere. Thus a tangent-lineation diagram is rather like a streak photograph of particles suspended in water flowing past a submerged hemispherical window. Note, however, that the true trend of a tangent lineation is not preserved by either equal-angle or equal-area projection; thus the angle between the tangent lineation and the north direction on the tangent-lineation diagram is in general a distortion of the true trend of the lineation.

Such diagrams are also referred to in a more specific sense as 'slip-linear diagrams' (e.g. Goldstein & Marshak 1988). Tangent-lineation diagrams, however, are not restricted to plotting slip lineations, but can be used to plot any data for which a lineation and the plane in which it lies are both important, such as stretching lineations in foliations or fold axes in axial surfaces.

ANALYSIS OF LINEATIONS FORMED DURING PROGRESSIVE SIMPLE SHEAR

We assume that slickenlines are everywhere parallel to the direction of instantaneous displacement across each local shear plane. This direction is also necessarily the direction of maximum rate of shear on that plane. We interpret these directions in terms of the macromotion in the fault zone by focusing attention on a single rigid block from the penetratively fractured rock mass in the fault zone, and we imagine that it is surrounded by a uniform continuum (Fig. 1). The deformation of the continuum is the macromotion, which in effect describes the averaged motion of the mass centroids of all the other blocks making up the rock. We then assume that the orientation of the maximum rate of shear of the continuum across the faces of the rigid block defines the orientation of the slickenlines that develop.

The macromotion is a deformation defined by the macrovelocity gradient tensor, which has a symmetric part, the instantaneous strain rate or the deformation rate, and an antisymmetric part, the macrospin. The direction of maximum rate of shear of the continuum on any surface of the rigid block is the maximum tangential component of the macrovelocity gradient tensor on that surface (Twiss *et al.* 1989, and in preparation). We assume this direction is, on the average, the direction of the slickenlines that form during the deformation.

The microspin defines the rotation rate of the rigid block and the local shear planes that make up its surface. In principle, the microspin can be an independent component of the motion, and we can therefore choose to consider any relationship between the microspin and the macrospin. We illustrate the principles for determining the shear sense from curved slickenfibers using the model of macroscopic progressive simple shear during which the microspin equals the macrospin (Willis 1977, has made an interesting theoretical and experimental study of the rotation rate of rigid blocks of different shapes in a fluid undergoing progressive simple shear).

Figure 3 shows two frames from a macroscopic progressive simple shear of a continuum during which a macroscopic square in the continuum is sheared into a parallelogram, and a macroscopic circle is deformed into a finite-strain ellipse. Microspin of a rigid octahedral block embedded in the continuum results in a clockwise rotation of the block as shown. Several characteristics are significant to the development of our interpretation.

(1) The deformation is non-coaxial, which means that the principal axes of finite strain e_k rotate with respect to those of the incremental strain ε_k, which themselves are parallel to the principal axes of instantaneous strain rate $\dot{\varepsilon}_k$ (Fig. 3). Local shear planes undergo rigid rotation in the same sense, along with the rigid block. Because the microspin equals the macrospin, the rotation rate of the blocks given by the microspin reflects the monoclinic symmetry of the macromotion.

(2) The axis of microspin is parallel to the intermediate principal axis of the instantaneous strain rate tensor $\dot{\varepsilon}_2$ and perpendicular to the plane of monoclinic symmetry for the macromotion (Figs. 1 and 3).

(3) The intersection of the monoclinic symmetry plane with the macroscopic shear plane is the macroscopic slip direction. The symmetry plane also contains the maximum and minimum instantaneous strain rate axes $\dot{\varepsilon}_1$ and $\dot{\varepsilon}_3$ (Figs. 1 and 3).

If the microspin is equal to the macrospin, the directions of maximum rate of shear on arbitrarily oriented local shear planes depend only on the ratio $D = (\dot{\varepsilon}_2 - \dot{\varepsilon}_3)/(\dot{\varepsilon}_1 - \dot{\varepsilon}_3)$ (Twiss *et al.* in preparation). For progressive simple shear, $\dot{\varepsilon}_2 = 0$ and $\dot{\varepsilon}_1 = -\dot{\varepsilon}_3$, giving $D = 0.5$. This value of D actually characterizes all pro-

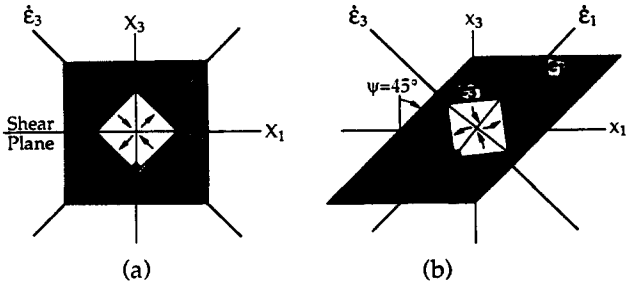

Fig. 3. Progressive simple shear, a non-coaxial deformation. Principal instantaneous strain rate axes $\dot{\varepsilon}_1$, $\dot{\varepsilon}_2$ and $\dot{\varepsilon}_3$ are constant in orientation, and principal axes of finite strain e_1, e_2 and e_3 rotate with respect to them. A rigid octahedral block (cf. Fig. 1) rotates at a rate given by the microspin, whose components equal the macrospin components. Symmetry plane for monoclinic motion is parallel to diagram, and the axis of microspin is perpendicular to diagram and parallel to $\dot{\varepsilon}_2$. Curved arrows on faces of octahedral block indicate expected slickenline orientations resulting from the motion (cf. Fig. 1). Intersection of symmetry plane and plane of faulting is parallel to slip direction.

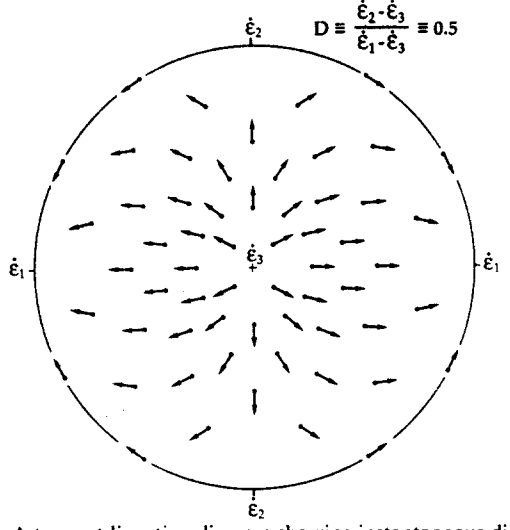

Fig. 4. A tangent-lineation diagram showing instantaneous directions of maximum rate of macroscopic shear on a distribution of local shear planes for the case of simple shear when microspin equals macrospin (lower-hemisphere, equal-angle projection).

gressive, plane strain, constant volume deformations. Values in the range $0 \leq D < 0.5$ characterize progressive, constrictional, constant volume deformation; and values in the range $0.5 < D \leq 1$ characterize progressive, flattening, constant volume deformation.

On a tangent-lineation diagram, we plot the directions of the instantaneous maximum rate of shear for a set of local shear planes that has a uniform distribution of orientations. For $D = 0.5$, the pattern of tangent lineations has orthorhombic symmetry (Fig. 4) and is the same as the pattern for the directions of maximum resolved shear stress.

A finite increment of deformation, however, includes a finite rigid rotation of the local shear planes because of the microspin. The rotation occurs about the unique microspin axis, which is parallel to $\dot{\varepsilon}_2$ (Fig. 1). As a local shear plane undergoes a progressive rigid rotation during progressive macroscopic simple shear, the shear direction of the continuum across the plane continually changes, as can be seen by imagining a shear plane pole rotating across the tangent-lineation diagram in Fig. 4. Thus in general, the newest slickenline to develop has an orientation that differs from both the original and the rotated orientations of the initial slickenline. The only exceptions are for the set of local shear planes whose normals are perpendicular to the microspin axis. Because new orientations of slickenline continuously develop on the local shear plane as it progressively rotates, a curved slickenline results. At present we consider only the oldest and the youngest orientations.

Figure 5(a) is a tangent-lineation diagram for a macroscopic shear angle of approximately $\psi = 19°$ (cf. Fig. 3b where $\psi = 45°$) showing the orientation pattern of the oldest slickenlines (small arrows) and the youngest slickenlines (large arrows) for each plane in an approximately uniform distribution of local shear plane orientations. The diagram was computed from theoretical equations developed by Twiss *et al.* (1989, and in preparation). All these planes have rotated from different initial orientations, at which they acquired the oldest slickenlines, to their final orientations, at which they acquired the youngest slickenlines. They have rotated from right to left across the diagram on small circles about the microspin axis, which is parallel to $\dot{\varepsilon}_2$. The angular difference between each pair of arrows indicates the amount of curvature the slickenlines would show on

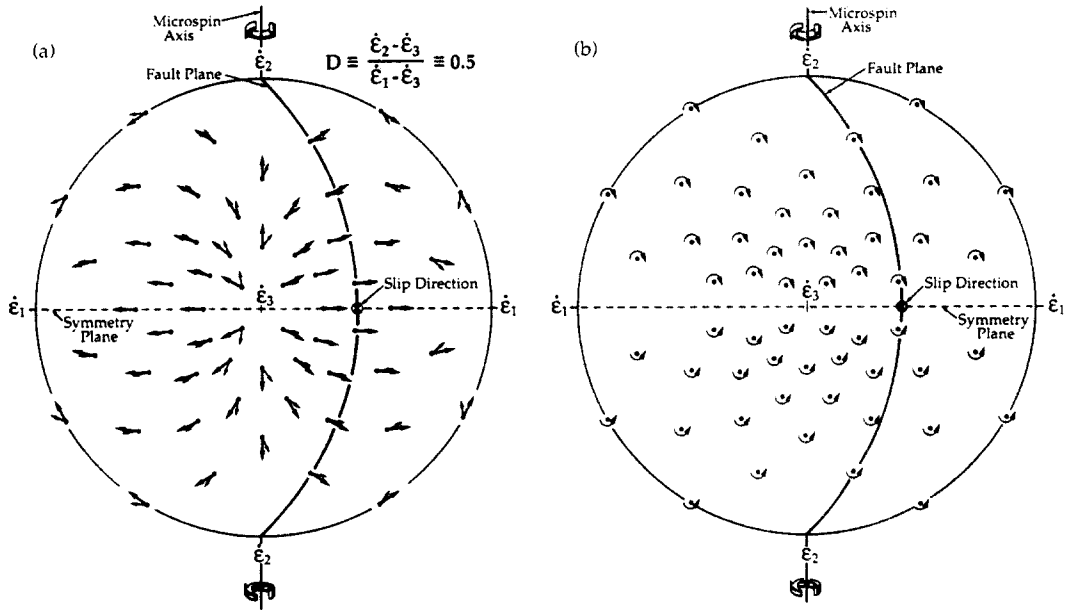

Fig. 5. After a finite increment of shear, local shear planes are rotated, and tangent-lineation diagram becomes monoclinic. Lineation pattern is shown after simple shearing through an angle $\psi = 19°$ (cf. Fig. 3 where $\psi = 45°$) (lower-hemisphere, equal-angle projections). (a) Orientations for oldest rotated slickenlines are shown by short arrows, and for youngest slickenlines by long arrows. The unique plane of monoclinic symmetry is parallel to $\dot{\varepsilon}_1$–$\dot{\varepsilon}_3$ plane, and microspin axis is parallel to $\dot{\varepsilon}_2$. (b) Constructing an arcuate arrow about the local shear plane pole from the orientation of youngest slickenline to oldest clearly defines symmetry of slickenline curvature. Sense of rotation about microspin axis is same as sense of curvature of slickenlines about local shear plane poles that lie in same field as microspin axis.

a given local shear plane. That amount varies with the orientation of the plane and depends on the relation between the microspin and the macrospin as well as on the total amount of macrodeformation. The pattern of the tangent-lineation diagram is now monoclinic, with the symmetry plane normal to the microspin axis and to $\dot{\varepsilon}_2$.

The symmetry of the pattern is clearer if we replace each pair of arrows in Fig. 5(a) with an arcuate arrow about the pole to the local shear plane to show the curvature sense (clockwise or counterclockwise) from *youngest to oldest* slickenline orientations (Fig. 5b). This convention for indicating the sense of curvature defines the sense of rotation of the local shear plane and is opposite to the growth direction of the slickenline (see Fig. 6 and associated discussion). The curvature sense thus defined is different on planes whose normals are on opposite sides of the symmetry plane for the macroscopic simple shear. From this pattern, therefore, we can immediately identify the symmetry plane, because that plane separates the data into fields of opposite curvature sense.

DETERMINING SHEAR SENSE OF A SHEAR ZONE

Although the analysis above is based on progressive simple shear, the same features would be characteristic of any deformation with monoclinic symmetry. Thus we can deduce a general technique for inferring shear sense from curved slickenlines.

In the field, we measure the orientation of the local shear plane and, looking down on the plane, record the sense of curvature (clockwise or counterclockwise) *from the youngest to the oldest* orientation of slickenline on that plane. We plot the shear plane pole on a spherical projection using a distinct symbol according to whether the slickenline on that plane shows clockwise or counterclockwise curvature sense. (In Fig. 10 we use dots and plusses to indicate clockwise and counterclockwise curvature sense, respectively.) The plane that best separates the data into two fields of opposite curvature sense is the symmetry plane for the macroscopic deformation (cf. Figs. 5b and 10). The axis of microspin is normal to the symmetry plane. The sense of rotation about that axis, looking down its plunge, is the same as the curvature sense plotted about the poles to shear planes that lie in the same field as the microspin axis (Fig. 5b).

If the orientation of the fault zone is plotted as a great circle on the same diagram, the macroscopic slip direction is parallel to the intersection of that great circle with the symmetry plane (Fig. 5; cf. Fig. 1). The rotation sense about the microspin axis defines the sense of shear in the fault zone.

INTERPRETATION OF SLICKENFIBER GROWTH

In order to determine the correct curvature sense for a curved slickenline, we must be able to distinguish the youngest from the oldest end of the slickenline. For

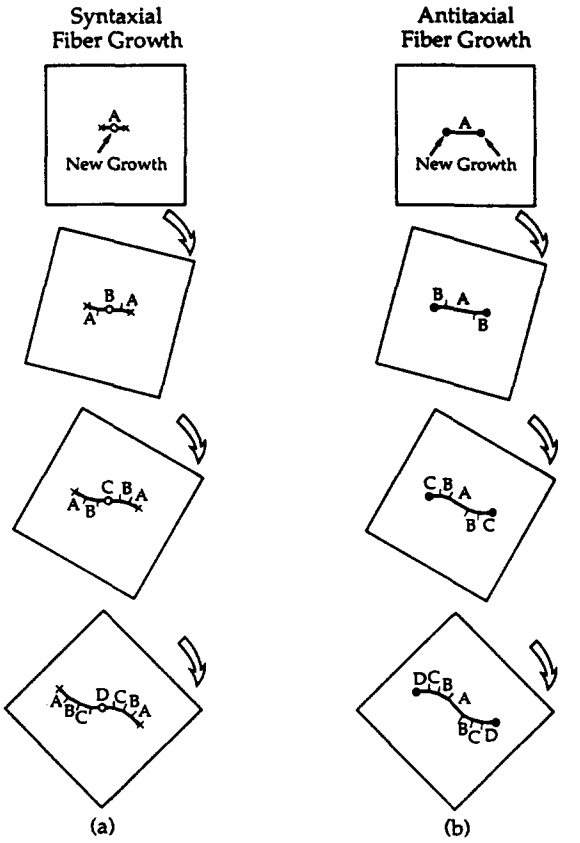

Fig. 6. Patterns of slickenfiber growth on a local shear plane rotating clockwise, assuming equal increments of growth alternating with equal increments of rotation. New fiber growth occurs at the point labeled with open circle. Each fiber is attached to opposite wall of local shear plane at point labeled ×. Age of fiber segments decreases from A (oldest) to D (youngest). (a) Syntaxial fiber growth. (b) Antitaxial fiber growth.

slickenfibers, we must therefore know whether the growth has been syntaxial or antitaxial (Durney & Ramsay 1973, Ramsay 1980, Ramsay & Huber 1983). Fibers that grow syntaxially increase in length by growth at a medial surface between the fracture walls, and an optical discontinuity in the fibers is evident across this surface. The fibers have the same composition as minerals in the wall rock and show optical continuity with those mineral grains. Fibers that grow antitaxially increase in length by growth at the interface between the fiber and both walls of the fracture. Small inclusions of wall rock material are commonly contained within the fibrous fracture filling and may define a distinct medial surface, but the fibers are optically continuous across the medial surface.

Figures 6(a) & (b) show the difference in curvature of the fibers that would develop for these two modes of fiber growth. The models assume constant increments of growth in a constant orientation alternating with equal increments of rotation. Segments of growth are labeled in alphabetical order, so that segments labeled 'A' are the oldest. New growth occurs at the points labeled with open circles, and fibers are connected to opposite fracture walls at the two points labeled with an '×'. In the antitaxial case, the circles and ×s are superimposed (Fig. 6b).

The sense of curvature from the youngest segment

(D) to the oldest segment (A) is the same (clockwise) in both cases and for both halves of the fiber, although the curvature of the whole fiber defines an 'S' in one case (Fig. 6a) and a 'Z' in the other (Fig. 6b). Thus observation of slickenfibers in the petrographic microscope might be necessary in order to be confident of the curvature sense recorded in the field.

APPLICATION TO THE FEATHER RIVER PERIDOTITE

The Feather River Peridotite is an ultramafic body in the northern Sierra Nevada of California. It is bounded on both the east and west sides by fault zones along which the body is completely serpentinized and extensively sheared (Fig. 7). The fault zones are part of an extensive system of faults commonly grouped together as the Foothills fault system, although different segments of this fault system may have different tectonic histories and significance. Within this system, the Feather River Peridotite occupies the Melones fault zone. Like many sheared serpentinites, the rock is characterized by a multitude of fractures that have a wide range of orientations and are covered by slickenfibers. Most slickenfibers are straight, although two intersecting sets of slickenfibers on the same surface are fairly common; curved slickenfibers (Fig. 8), although not abundant, are common enough to provide a significant amount of data. Observed amounts of curvature on different local shear planes is highly variable, but ranges up to a maximum of about 90°. Although the fibers are serpentine and the walls of the shear fractures are serpentinized, the mode of growth is antitaxial (Fig. 9).

The tectonic significance and history of the two fault zones bounding the peridotite body has been the subject of considerable debate. Gefell (1989) made a detailed analysis of the shear sense indicators along the margins of the peridotite, both in the peridotite and in the adjacent rocks (Gefell *et al.* 1989). The curved slickenfiber technique was applied to determine the sense of shear of a late brittle phase of deformation along the fault zones.

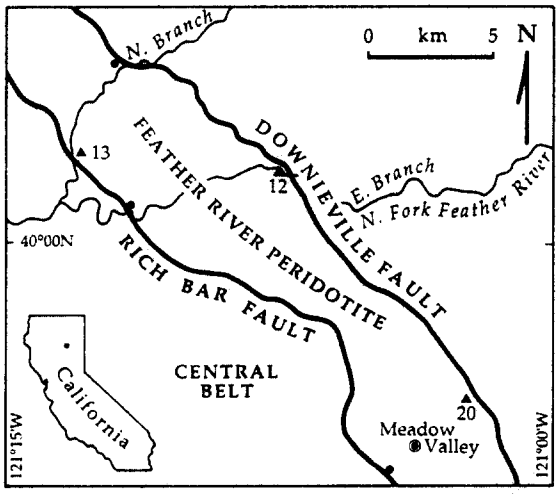

Fig. 7. Index map of California and study area within Feather River Peridotite. Areas from which data in Fig. 11 were obtained are indicated by triangles; other data localities are indicated by dots.

The data from the three locations that provided well-defined results (Fig. 7, triangles) are shown in Fig. 10. One of the useful data sets is from the west side of the peridotite (Fig. 10a) and two are from the east side (Figs. 10b & c). Other locations (Fig. 7, dots) yielded ambiguous or uninterpretable data, which we discuss in the next section. Each diagram in Fig. 10 is a plot of local shear plane poles, for which we have used a different symbol according to whether the slickenfibers on the plane show a curvature sense that is clockwise (dots) or counterclockwise (plusses), where curvature sense is determined from youngest to oldest orientation. Using these symbols allows easier visual interpretation of the diagram than the curved arrows shown in Fig. 5(b), but the significance is the same.

In Fig. 10(a), we can visually locate a plane that provides a good separation of the data into fields of opposite curvature sense. The comparable plane is less well constrained in Fig. 10(b) and poorly constrained in Fig. 10(c), where one curvature sense is not well represented. For Fig. 10(c), we chose a plane that marks a boundary for the majority of the data having the same curvature sense and that is as consistent as possible with the few data available of the opposite curvature sense.

An imperfect separation of data that lie immediately along the plane is easily accounted for by inaccuracies of measurement and minor inhomogeneities in deformation. Apart from these data, each diagram contains one or two data points that unequivocally plot in the wrong field. We discuss the possible origins of such data in the next section.

We interpret the plane that separates the data into fields of opposite curvature sense to be the symmetry plane for the macroscopic deformation, and the pole to that plane to be the axis of microspin. The rotation sense about the microspin axes is clockwise (heavy dots) in Figs. 10(a) & (b), and counterclockwise (heavy plusses) in Fig. 10(c). This rotation sense is the same as the curvature sense about the local shear plane poles that plot in the same field as the microspin axis.

The solid great circle in each diagram (Fig. 10) indicates the approximate regional orientation of the Melones fault zone in the area of study (cf. Fig. 7). In principle, the microspin axis should be parallel to the fault zone (Fig. 1), a relationship which holds true for Fig. 10(a), is close for Fig. 10(c), and is only approximate for Fig. 10(b). The intersection of the macroscopic shear zone orientation with the symmetry plane defines the approximate direction of macroscopic slip on the fault zone. Thus Figs. 10(a) & (b) indicate oblique-slip plunging to the southeast, and Fig. 10(c) indicates essentially dip-slip. The rotation senses inferred for the microspin axes are all consistent with dextral-normal (Figs. 10a & b) or normal (Fig. 10c) slip.

The two data sets that best constrain the symmetry plane (Figs. 10a & b) give very consistent results of southeast dextral-normal slip on the fault zone. The

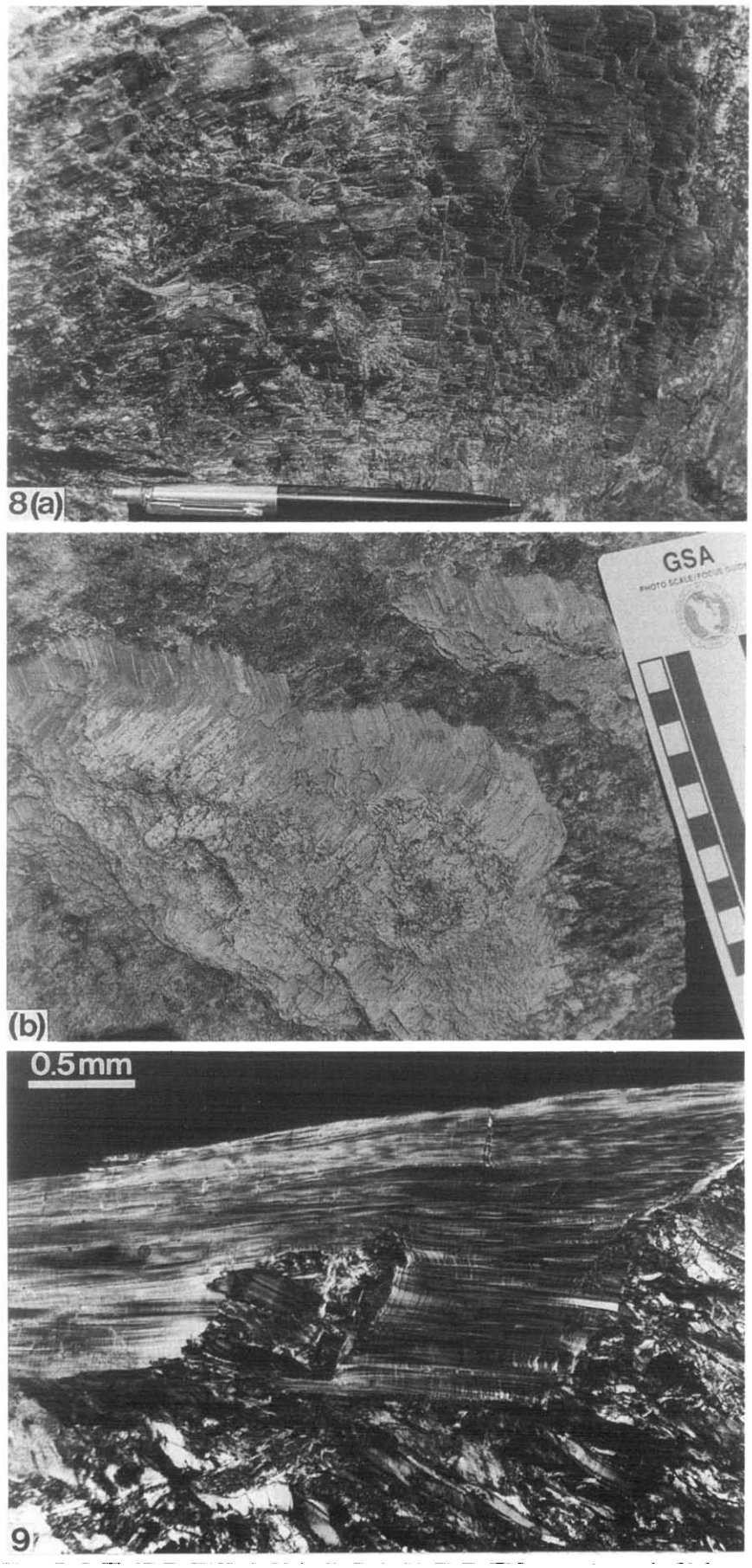

Fig. 8. Serpentine slickenfibers from Feather River Peridotite. (a) A smoothly curved slickenfiber lineation. (b) A sharply curved slickenfiber lineation.

Fig. 9. Photomicrograph of serpentine slickenfibers in a pull-apart along a local shear plane, showing antitaxial character of fibers. Growth lines can be discerned at a high angle to fibers.

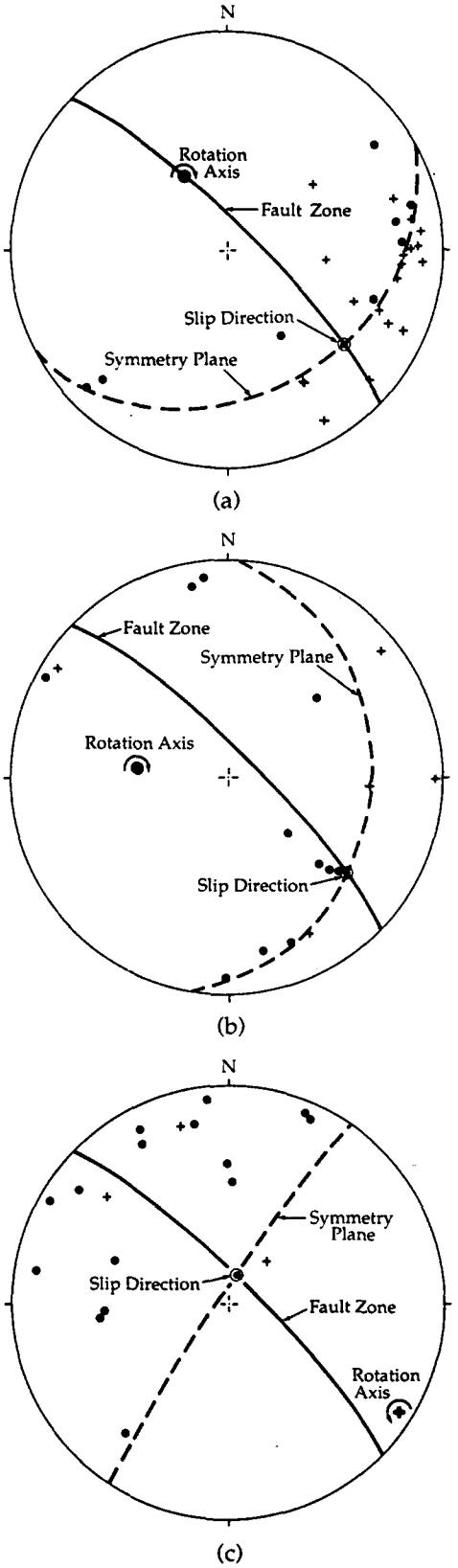

Fig. 10. Curved slickenfiber data from west and east margins of Feather River Peridotite (cf. Fig. 7). Data points are poles to local shear planes which are plotted as dots if slickenfiber curvature on the plane is clockwise, and as crosses if curvature is counterclockwise. Slickenfiber curvature is from youngest to oldest part of the fiber, looking down on plane. Dashed planes are inferred symmetry planes for macroscopic motion. Solid plane indicates approximate orientation of the Melones fault zone in this region. Inferred microspin axes, rotation senses, and slip directions are labeled (lower-hemisphere, equal-area projections). (a) Area 13: 26 points. Dextral-normal oblique-slip. (b) Area 20: 15 points. Dextral-normal oblique-slip. (c) Area 12: 18 points. Normal dip-slip.

third data set (Fig. 10c) provides only poor constraint of the symmetry plane which may account for the difference in slip direction. Thus we infer the most probable geometry of faulting for the area to be dextral-normal slip, as shown diagrammatically in Fig. 11. On the NW-striking, steeply NE-dipping fault zone, the slip direction plunges to the southeast, and the clockwise rotation sense on the microspin axis indicates dextral-normal oblique slip.

DISCUSSION

The symmetry of the velocity field for progressive simple shear is monoclinic, characterized by one mirror plane of symmetry normal to the shear plane and parallel to the slip direction, and one two-fold axis of rotational symmetry normal to the symmetry plane (Fig. 1). We expect, therefore, that structures such as slickenlines that record an aspect of the displacement field could preserve this symmetry. In nature, the local shear planes commonly have a preferred orientation. Thus the actual plots of field data are not themselves necessarily monoclinic (Fig. 10) because they show only a portion of the entire monoclinic pattern in Fig. 5(b). Nevertheless, because the sense of curvature of slickenlines on local shear planes changes across the symmetry plane, we can infer the orientation of this plane from a diagram that itself does not actually display the symmetry.

Observations made in the field are not completely in accord with the predictions of the model. For example, straight and crossing slickenfibers are more abundant than curved slickenfibers. Some curved slickenfibers are smoothly curved (Fig. 8a), but others are sharply curved (Fig. 8b). Moreover, the results from the three different localities show quite different orientations of the symmetry plane (Fig. 10), the microspin axis does not, in every case, lie in the fault plane, and results from some localities are uninterpretable. The model on which the analysis is based assumes that the deformation is homogeneous and the motion is steady, which is certainly over-simplified. Deviations from these assumptions probably account for differences between the model and observation.

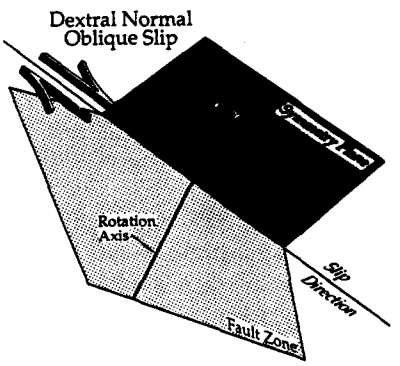

Fig. 11. Generalized geometry of dextral-normal shear inferred from curved serpentine slickenfibers in Feather River Peridotite along Melones fault zone.

The abundance of straight slickenfibers that we observed may be explained in part by the fact that for a large range of shear plane orientations, the angle between young and old fiber orientations is quite small (Fig. 5a) and might not be detectable in the field. Beyond that, however, the deviation can be accounted for by a more realistic model of the deformation. The deformation of a pervasively fractured body can be visualized as if it were a very coarsely granular material in which the 'grains' are the blocks of rock that are bounded on all sides by fractures. Deformation is accommodated by sliding on the fracture surfaces, or 'grain boundaries', and this sliding is recorded by the slickenlines. The freedom of the blocks to rotate, however, is restricted because they are angular and tightly packed. Thus we cannot expect the macroscopic deformation or the microspin to be homogeneous and steady on a small scale.

For slickenlines to be curved, they must grow over a period of time sufficient for significant rotation of the local shear planes to occur. Slip on local shear planes, and thus growth of the slickenlines, however, does not have to be continuous throughout the entire deformation. Thus without free rotation, straight lineations could easily form. Because of the inhomogeneity, changes in slip direction on local shear planes may be discontinuous rather than gradual, resulting in crossing lineations and causing some lineations to be sharply instead of smoothly curved.

The reliability of orientations inferred for the symmetry planes, of course, depends on the quality of the data, and if the symmetry planes are poorly constrained, results from different data sets will not agree. Differences in the orientations of symmetry planes from different localities may be real, however, because even on the macroscopic scale, we cannot realistically expect the deformation to be homogeneous and steady. Irregularities in the geometry of the fault zone and its boundaries (Fig. 7), for example, require a change in the geometry of the deformation at any given material point as the shearing progresses. If the local orientation of shearing changes during the deformation, the total deformation in general becomes triclinic, and the monoclinic plane of symmetry is destroyed. Such deformation would yield uninterpretable data from curved slickenlines. Thus we might expect instances in which the application of the curved slickenfiber technique would give ambiguous or uninterpretable results, as indeed we found in the analysis of the Feather River Peridotite. Plotting all the data in Fig. 10 together in a regional composite plot, for example, would clearly destroy any obvious symmetry plane.

Smoothly curved slickenfibers imply that the history of fiber growth was continuous and therefore that the recorded deformation was a single continuous episode rather than the result of two or more differently oriented superposed deformations. The fact that the symmetry plane of the curved slickenfiber pattern is susceptible to destruction by changes in the geometry of the deformation has both positive and negative implications. On the negative side, it means that the technique is not very robust. On the positive side, it means that it is highly unlikely that interpretable patterns of slickenfiber curvature could result from a progressive change in the orientation of the principal instantaneous strain rate axes, because such changes, reflecting changing tectonic conditions, would most likely destroy the monoclinic symmetry.

The clearest results should come from local areas where the deformation most closely approximates a homogeneous and steady condition, which may be areas in which the deformation has been relatively short-lived. In such areas the local geometry of the deformation might deviate somewhat from the average for the fault zone. In Fig. 10, we plot a single orientation for the fault zone. In fact, the actual fault contact is poorly exposed and the orientation of the fault in local areas is not closely constrained. Significant variations in trend of the fault are suggested by the surface trace shown in Fig. 7. These considerations could account for the different observed symmetry planes and for the cases in which the inferred axis of local rotation is not exactly parallel to the regional orientation of the fault zone (Figs. 10b & c).

If crossing sets of slickenlines developed because of discontinuous shear-induced rotation or discontinuous local shear, they also could be used in the same manner as the curved slickenlines to infer shear sense in the shear zone. For slickenfibers, however, the interpretation is less secure because the genetic relationship between the young and old slickenfibers is less definite for crossing slickenfibers than it is for curved slickenfibers. Growth of a new set of crossing fibers does not necessarily begin from the youngest ends of the earlier fibers, thereby making ambiguous any superposition relationship between the crossing fibers. Crossing sets of slickenlines could also be due to a superposition of two different deformations, in which case they would probably yield uninterpretable results because it is unlikely that a symmetry plane would exist. Our attempts at interpreting crossing slickenfiber sets so far have been unsuccessful.

The abundance of straight slickenlines suggests the possibility of interpreting the data simply in terms of an orthorhombic tangent-lineation diagram such as in Fig. 4. An iterative program written by J. Angelier was used to calculate the orientation of the principal stress directions from straight slickenline data, assuming the slickenlines are parallel to the directions of maximum resolved shear stress on the local shear planes. The program provides unstable results and leaves as many as 40% or 50% of the data unsatisfactorily accounted for. Using Angelier's program to separate the data into two distinct populations, for which principal stress axes are independently determined, also gives unstable and inconsistent results.

We conclude that rotation of the local shear planes with their lineations has produced sufficient reorientation that the interpretation of the data in terms of one or two orthorhombic tensor orientations is problematical. Thus trying to infer slip direction by inspection of a

tangent-lineation diagram of the data would also be unreliable or impossible. The curved slickenfiber technique, however, provides a consistent means of interpreting non-coaxial bulk deformations. Furthermore, it can be applied in the field and does not require a complex computer analysis of the data.

Regional analyses of strain and stress orientations support our interpretation of late normal and normal-dextral motions along the bounding faults of the Feather River Peridotite. Eddington *et al.* (1987) have deduced from fault slip geometries in the northeastern Sierra Nevada and in northwestern Nevada that the region has undergone E–W extension between 10^7 and 10^4 years ago. This extension has imposed a normal component of slip on many reactivated Mesozoic-age reverse faults of the Foothills fault system, including the Melones fault zone (Alt *et al.* 1977).

This process probably is ongoing. The present-day least principal horizontal stress direction across the northern Sierra Nevada trends about 090°, as evidenced by seismic moment tensors (Eddington *et al.* 1987), focal mechanisms and borehole breakout data (Zoback & Zoback 1980). East–west extension should produce slip vectors that trend about 090° or 270° on pre-existing faults (Zoback & Zoback 1980), causing NW-striking faults to slip obliquely with normal and dextral components. Focal mechanisms (Wong & Savage 1983) and miners' observations of the fault displacement of piercing points defined by stream channels in the northern Sierra Nevada (Cassaway 1899) bear out this prediction, and corroborate our results.

CONCLUSION

We conclude that our technique for analysing curved slickenlines that form by progressive lengthening during deformation can indicate the slip direction and the shear sense in brittle shear zones where slickenlines have a wide diversity of orientations that are inconsistent with direct inference of slip direction and shear sense. It therefore provides a valuable addition to the existing techniques for determining shear sense in shear zones. In the Feather River Peridotite, at least, the detailed analysis of local areas appears more fruitful than regional syntheses. Probably because of inhomogeneous and unsteady deformation, however, the solutions in some cases are ambiguous or uninterpretable.

Acknowledgements—We are grateful for financial support of this research, which was provided in part by a grant to R. J. Twiss from the Committee on Research of the Academic Senate, University of California at Davis, and by grants in aid of research to M. J. Gefell from the Geological Society of America, the American Association of Petroleum Geologists, and the Durrell Fund awarded by the Geology Department, University of California at Davis. We thank G. Protzman and S. Hurst for the use of their programs by which we calculated the diagrams in Figs. 4 and 5(a). The presentation of these ideas benefited greatly from the suggestions of W. D. Means and an unidentified reviewer. Technical support was provided by the Geology Department at U.C. Davis, and we thank Janice Fong for drafting the figures.

REFERENCES

Alt, J., Schwartz, D. & McCrumb, D. 1977. *Earthquake Evaluation Studies of the Auburn Dam Area. 3. Regional Geology and Tectonics*. Woodward-Clyde Consultants, San Francisco.

Angelier, J. 1979. Determination of the mean principal directions of stresses for a given fault population. *Tectonophysics* **56**, T17–T26.

Angelier, J. 1984. Tectonic analysis of fault slip data sets. *J. geophys. Res.* **89**, 5835–5848.

Berthé, D., Choukroune, P. & Jegouzo, P. 1979. Orthogneiss, mylonite and non-coaxial deformation of granites: the example of the South Armorican Shear Zone. *J. Struct. Geol.* **1**, 31–42.

Bott, M. H. P. 1959. The mechanics of oblique slip faulting. *Geol. Mag.* **96**, 109–117.

Cassaway, A. D. 1899. The Magalia, California, drift mine. *Min. Sci. Press* **78**(114), 372.

Durney, D. W. & Ramsay, J. G. 1973. Incremental strains measured by syntectonic crystal growth. In: *Gravity and Tectonics* (edited by DeJong, K. A. & Scholten, R.). John Wiley and Sons, New York, 67–96.

Eddington, P. K., Smith, R. B. & Renggli, C. 1987. Kinematics of Basin and Range intraplate extension. In: *Continental Extensional Tectonics* (edited by Coward, M. P., Dewey, J. F. & Hancock, P. L.). *Spec. Publs geol. Soc. Lond.* **28**, 371–392.

Etchecopar, A., Vasseur, G. & Daignieres, M. 1981. An inverse problem in microtectonics for the determination of stress tensors from fault striation analysis. *J. Struct. Geol.* **3**, 51–65.

Gefell, M. J. 1989. Shear sense for the bounding faults of the Feather River Peridotite, northern Sierra Nevada, California. Unpublished M.S. thesis, Geology Department, University of California at Davis.

Gefell, M. J., Twiss, R. J. & Moores, E. M. 1989. Ductile and brittle shear sense for the "Melones Fault Zone", northern Sierra Nevada, California. *Geol. Soc. Am. Abs. w. Prog.* **21**, 83.

Goldstein, A. & Marshak, S. 1988. Analysis of fracture array geometry. In: *Basic Methods of Structural Geology* (written and edited by Marshak, S. & Mitra, G.). Prentice-Hall, Englewood Cliffs, New Jersey, 249–267.

Hancock, P. L. 1985. Brittle microtectonics: principles and practice. *J. Struct. Geol.* **7**, 437–457.

Hansen, E. C. 1971. *Strain Facies*. Springer, New York.

Hoeppener, R. 1955. Tektonik im schiefergebirge eine einfuhrung. *Geol. Rdsch.* **44**, 26–58.

Lister, G. S. & Snoke, A. W. 1984. S–C mylonites. *J. Struct. Geol.* **6**, 617–638.

Marshak, S., Geiser, P. A., Alvarez, W. & Engelder, T. 1982. Mesoscopic fault array of the northern Umbrian Apennine fold belt, Italy: geometry of conjugate shear by pressure-solution slip. *Bull. geol. Soc. Am.* **93**, 1013–1022.

Means, W. 1987. A newly recognized type of slickenside striation. *J. Struct. Geol.* **9**, 585–590.

Passchier, C. W. & Simpson, C. 1986. Porphyroclast systems as kinematic indicators. *J. Struct. Geol.* **8**, 831–843.

Petit, J.-P. 1987. Criteria for the sense of movement on fault surfaces in brittle rocks. *J. Struct. Geol.* **9**, 597–608.

Platt, J. P. & Vissers, R. L. M. 1980. Extensional structures in anisotropic rocks. *J. Struct. Geol.* **2**, 397–410.

Ramsay, J. 1980. The crack-seal mechanism of rock deformation. *Nature* **284**, 135–139.

Ramsay, J. & Huber, M. 1983. *The Techniques of Modern Structural Analysis, Volume* 1: *Strain Analysis*. Academic Press, New York.

Simpson, C. & Schmid, S. 1983. An evaluation of the criteria to deduce the sense of movement in sheared rocks. *Bull. geol. Soc. Am.* **94**, 1281–1288.

Twiss, R. J., Protzman, G. M. & Hurst, S. D. 1989. Interpretation of slickenside lineation patterns in terms of the velocity gradient tensor and finite deformation. *Geol. Soc. Am.* 1989 *Annual Meeting Abs. w. Prog.* **21**, A265.

Willis, D. G. 1977. Kinematic model of preferred orientation. *Bull. geol. Soc. Am.* **88**, 883–894.

Wong, I. & Savage, W. 1983. Deep intraplate seismicity in the western Sierra Nevada, central California. *Bull. seism. Soc. Am.* **12**, 391–394.

Zoback, M. L. & Zoback, M. 1980. State of stress in the conterminous United States. *J. geophys. Res.* **85**, 6113–6156.